



Published in final edited form as:

Biochemistry. 2015 August 11; 54(31): 4900–4908. doi:10.1021/acs.biochem.5b00388.

Structure based identification of inhibitors for the SLC13 family of Na⁺/dicarboxylate cotransporters

Claire Colas[†], Ana M. Pajor^{‡,*}, and Avner Schlessinger^{†,*}

[†]Department of Pharmacology and Systems Therapeutics, Tisch Cancer Institute, Icahn School of Medicine at Mount Sinai, New York, NY 10029

[‡]Skaggs School of Pharmacy and Pharmaceutical Sciences, University of California-San Diego, La Jolla, CA 92130-0718 (A.M.P)

Abstract

In mammals, citric acid cycle intermediates play a key role in regulating various metabolic processes, such as fatty acid synthesis and glycolysis. Members of the sodium dependent SLC13 transporter family mediate the transport of di and tricarboxylates into cells. SLC13 members have been implicated in lifespan extension and resistance to high fat diets, thus, they are emerging drug targets for aging and metabolic disorders. We previously characterized key structural determinants of substrate and cation binding for the human NaDC3/SLC13A3 transporter using a homology model. Here, we combine computational modeling and virtual screening with functional and biochemical testing, to identify 9 previously unknown inhibitors for multiple members of the SLC13 family from human and mouse. Our results reveal previously unknown substrate selectivity determinants for the SLC13 family, including key residues that mediate ligand binding and transport, as well as promiscuous and specific SLC13 small molecule ligands. The newly discovered ligands can serve as chemical tools to further characterize the SLC13 family or as lead molecules for future development of potent inhibitors for the treatment of metabolic diseases and aging. Our results improve our understanding of the structural components that are important for substrate specificity in this physiologically important family as well as in other structurally related transport systems.

Citric acid cycle (CAC) intermediates such as succinate, citrate, and malate are involved in regulating a variety of important metabolic processes in mammals, such as fatty acid synthesis and glycolysis.^{1–3} For example, citrate is a regulatory signal in the brain for sensing energy and nutrient availability.³ In humans, the transport of these di- and tri-carboxylates across the plasma membrane into cells is mediated through three sodium dependent transporters of the SLC13 family: hNaDC1 (SLC13A2), hNaDC3 (SLC13A3) and hNaCT (SLC13A5). Reduction of the activity of SLC13 homologs in *D. melanogaster*^{4, 5} and *C. elegans*^{6, 7} leads to increased lifespan and reduced fat storage. More recently, deletion of the mouse *slc13a5* (mNaCT) was shown to cause substantial metabolic

*avner.schlessinger@mssm.edu; apajor@ucsd.edu.

Supporting Information Available.

Ligand libraries for virtual screening, Figure S1, Table S1. This material is available free of charge via the Internet at <http://pubs.acs.org>.

changes, increased plasma citrate concentrations and resistance to the deleterious effects of a high fat diet.⁸ Thus, the SLC13 family members are emerging drug targets for metabolic disorders and aging.

The SLC13 family members have diverse tissue distribution and substrate specificities.⁹ For example, hNaDC1, found primarily in the renal proximal tubule and small intestine, is a low affinity transporter (K_m for succinate is 0.5 mM) of di- and tri-carboxylates ranging from four- to six-carbon molecules (e.g., succinate and citrate, respectively).¹⁰ Conversely, hNaDC3 is expressed in multiple tissues, including the kidney (basolateral membrane), liver, placenta, brain, choroid plexus, and eye.^{11, 12} hNaDC3 is a high affinity transporter (K_m for succinate ~20 μ M) that transports a broader range of substrates than hNaDC1, including dicarboxylates with longer or bulkier sidechains, as well as drugs such as succimer and the antioxidant glutathione.^{13, 14} In contrast, the liver and brain Na^+ /citrate transporter, NaCT, has a narrow substrate specificity with a preference for citrate.¹⁵ The mechanisms underlying the transport of the CAC intermediates, including the structural basis for the differential binding and transport specificity among the SLC13 members, are poorly understood.

Description of the substrate specificity determinants of the SLC13 transporters includes the identification of structural features such as charge, polarity, and shape, on the proteins' surface that determine differential binding and transport of small molecules ligands and ions. There is currently no known experimentally determined atomic structure for any of the human SLC13 family transporters; however, the structure of the bacterial homolog, the sodium dependent dicarboxylate transporter from *Vibrio cholerae* INDY (vcINDY) has been recently determined at atomic resolution.¹⁶ The vcINDY structure, which revealed a novel structural fold, represents an inward open conformation bound to a citrate and a sodium ion, and consists of two pseudo-symmetrical halves, indicating an "alternating access" transport mechanism, related to other structurally dissimilar transporter families (e.g., LeuT).¹⁷ vcINDY shares sequence identity of 33–35% with the mammalian SLC13 members and a conserved binding site. Furthermore, recent functional studies of vcINDY suggest an ion:substrate transport stoichiometry of 3:1, similar to those of hNaDC3 and hNaDC1,¹⁸ Recently, two structures of the same fold have been determined in a similar inward conformation,^{19, 20} but they are only distantly related to the mammalian SLC13 family (sequence identity of ~15%). Therefore, the vcINDY is the most suitable template to generate homology models of the human SLC13 transporters from human and mouse. We have previously described a homology model of hNaDC3, which revealed previously unknown structural features important for ligand and ion recognition.²¹ Residues that belong to the conserved Serine-Asparagine-Threonine (SNT) motifs were demonstrated by site-directed mutagenesis to mediate substrate and sodium binding in hNaDC3 (e.g., Ser143, Asn144, Thr485).

In this study, we use a combination of computational prediction and experimental validation to characterize multiple SLC13 family members from human and mouse, providing a more comprehensive description of the specificity determinants in this family. We constructed homology models of the human NaDC1 (hNaDC1), mouse NaDC1 (mNaDC1), mouse NaDC3 (mNaDC3) and human NaCT (hNaCT), and used virtual screening of various small

molecule libraries to predict inhibitors of these proteins. The top scoring hits were then tested experimentally using uptake kinetic measurements in cells. Finally, we discuss how the results of the study improve our understanding of the structural basis for substrate selectivity among the SLC13 family, and can promote the development of potential effective drugs targeting SLC13 members.

MATERIALS AND METHODS

Homology Modeling

We modeled three SLC13 family transporters (hNaDC1, mNaDC1 and mNaDC3), based on the X-ray structure of vcINDY (PDB ID: 4F35).¹⁶ We relied on a previously published alignment between hNaDC3 and vcINDY,²¹ and aligned the other SLC13 members based on multiple sequence alignment generated using the server PROMALS3D.²² We used MODELLER-9 v.14 to build 100 initial models for each target, which were assessed and ranked by the statistical potential Z-DOPE.²³ The models were built with non-protein atoms that were derived from the corresponding coordinates of the vcINDY structure. These non-protein atoms included a sodium ion (Na⁺), as well as atoms from citrate, a weak inhibitor of this protein.¹⁶ Moreover, although a second cation binding site has been previously proposed to be located in close proximity to the ligand,¹⁶ it has not been determined whether both ions are bound with high affinity in this conformation of vcINDY. In fact, in vcINDY, it has been suggested that this conformation represents a state where the second cation has already been released in the cytoplasm.¹⁶ Taken together, we hypothesized that models of human SLC13 members in this conformation are suitable for identifying new ligands via virtual screening. While other useful conformational states can be modeled using a variety of approaches such as relying on the pseudo-symmetry of the protein,²⁴ such models are less likely to be sufficiently accurate for structure-based ligand discovery.²⁵

The highest ranked models obtained Z-DOPE values ranging from -0.27 to -0.12 , suggesting that 50%–55% of their C α atoms are within 3.5 Å of their correct positions.²⁶ These top-scoring models were visually inspected in view of previous studies characterizing structure-function relationships among SLC13 members.⁹ Finally, the side chain of Thr236 of the mNaDC1 model was refined with Chimera²⁷ to face the binding pocket.

Virtual screening and ligand docking

OpenEye FRED (Fast Rigid Exhaustive Docking)²⁸ was used for all docking calculations. The transporter's binding site was prepared with the MAKE_RECEPTOR utility. We defined a box enclosing the binding site around the coordinates of the citrate derived from the X-ray structure of vcINDY, and the sodium ion was defined as part of the binding site.¹⁶ The docking poses were evaluated by the Chemgauss4 scoring function, which is based on the shape- and chemical-complementarity between the ligands and the binding site.²⁸ We docked three subsets from the ZINC database: the 'Drugs Now', 'Leads Now' and 'Fragments Now' subsets (2,726,001 compounds in total), against the hNaDC1 and hNaDC3 models and prioritized molecules for experimental testing based on visual analysis (*SI Text*).

Briefly, we compared the docking poses of the top 500 scoring ligands of each screen to those of known ligands in the models, as well as to the mode of interaction of citrate in the experimentally determined structure of vcINDY (Figure 1).¹⁶ In brief, eight molecules were initially tested (**1–8**, Table 1) based on the following considerations: i) we favored dicarboxylate compounds interacting with the N- or C-termini SNT motifs, which are highly important for function;^{9, 21, 29} ii) moreover, to explore non-trivial ligands and previously unknown modes of interaction with the transporters, we prioritized molecules that are predicted to interact with other key binding site residues. For example, Thr527 of hNaDC3 was suggested to participate in a network of interactions involving the substrate and a putative second Na⁺ ion;²¹ iii) finally, we selected molecules that contain novel scaffolds (e.g., aromatic rings). For example, molecules **1** and **3** included a toluene and a naphthalene group, respectively, that were predicted to form a hydrophobic interaction with a hydrophobic subpocket in hNaDC3 (constituted by helices TM9b, TM5b and HP_{out}) (Figure 3A). The selected compounds were then also docked in the mouse models.

Cell culture

Human embryonic kidney (HEK-293) cells (CRL-1573, American Type Culture Collection, Manassas, VA) were cultured in Dulbecco's Modified Eagle's Medium (DMEM) supplemented with 25 mM HEPES, 2 mM Glutamax, 1 mM Na-pyruvate, 0.1 mM non-essential amino acids, 10% heat-inactivated fetal calf serum, 100 U/ml penicillin, 100 µg/ml streptomycin at 37°C in 5% CO₂.³⁰ Cells were plated on poly-D-lysine-coated 96-well plates (BD Biosciences, San Jose, CA) at 0.6×10^5 cells per well and transfected with plasmids coding for SLC13 transporters using FuGene6 (Roche Applied Science, Indianapolis, IN) at a 3:1 ratio.

Transport assays

Uptakes of 2,3-[¹⁴C]succinate (52 mCi/mmol) or 1,5-[¹⁴C]citrate (112 mCi/mmol) (both from Moravek, La Brea, CA) were assayed 48 hours after transfection, also as described³⁰. The [¹⁴C]citrate was used for the citrate transporter, NaCT, because of low succinate transport activity. The sodium transport buffer contained in mM: 140 NaCl, 2 KCl, 1 MgCl₂, 1 CaCl₂, 10 HEPES, pH adjusted to 7.4 with 1 M Tris. Choline buffer contained equimolar cholineCl in place of NaCl. For the assays, each well was washed twice with choline buffer, then incubated with 50 µl sodium buffer containing ~10 µM [¹⁴C]succinate or [¹⁴C]citrate for 30 min at room temperature. The uptake assays were stopped and surface radioactivity removed with 4×1 ml washes of choline buffer. Cells were dissolved using Ultima Gold scintillation cocktail (Perkin Elmer), then the plates were counted directly using a Wallac Microbeta plate scintillation counter. For all experiments, counts in vector-transfected cells were subtracted from counts in SLC13 plasmid-transfected cells to correct for background.

Initial screens of inhibitors were done using concentrations of 500 µM. The inhibitor stock solutions were made to 50 mM in DMSO and control groups received DMSO only. The final concentration of DMSO was 1%. For subsequent measurements of IC₅₀ values, a range of stock solutions was made so that equal volumes of DMSO were added to each well. For the initial screen, all inhibitors were preincubated 12 min in sodium buffer, then plates were washed and radioactive solution with inhibitor was added.³¹ However, we found that

inhibition does not require preincubation (results not shown) and, therefore, subsequent IC₅₀ measurements were done without the preincubation. IC₅₀ values were determined by fitting the data to a four-part logistic curve (SigmaPlot 10.0, Systat Software Inc., San Jose, CA).

Statistics

Duplicate or quadruplicate measurements were made for each data point. The experiments were repeated with at least three different batches of transfected cells from different passage numbers. Significant differences between groups were identified by Student's t-test or ANOVA with P<0.05.

Chemicals

All of the compounds were purchased from commercial vendors. Compounds 1,5,6,12 were from ChemBridge (San Diego, CA); compounds 2,4 were from Vitas-M-lab (Narva, Estonia); Compounds 3, 10, 11, 13 were from Sigma-Aldrich (St. Louis, MO); Compound 7 was from Matrix Scientific (Columbia, SC); Compounds 8, 9 were from Enamine (Ukraine).

RESULTS

Structural models of the SLC13 members

The models of hNaDC1, mNaDC1 and mNaDC3 were built using MODELLER, based on the X-ray structure of vcINDY as a template¹⁶ (Figure 1) (Materials and Methods), similarly to our previously described hNaDC3 model.²¹ The vcINDY template structure represents an inward open conformation of the transporter bound to citrate, a weak inhibitor of this protein. Notably, previous studies proposed that vcINDY transports solutes via elevator-type mechanism similar to that of Glt_{ph}¹⁸, suggesting that the structure of the substrate binding pocket is similar in distinct conformational states of the transporter. Indeed, our previous study confirmed that substrate binding residues predicted from this conformation affect transport activity.²¹

The SLC13 models consist of the entire transmembrane domain of the proteins, including 11 helices and two hairpin loops, termed HP_{in} and HP_{out}. The tips of these hairpins support two Serine-Asparagine-Threonine (SNT) motifs that interact with the substrate and at least one Na⁺ ion. These SNT motifs, as well as the majority of the other binding site residues, are highly conserved within the SLC13 family, with some variations in the following two positions (Table 1). Position 1 is located in close proximity to the C-terminal SNT motif, and it can be an alanine (in hNaDC1, hNaDC3, and mNaDC3), a glycine (hNaCT), or a threonine (mNaDC1); Position 2 is the third residue of the C-terminal SNT motif can be a threonine, a Valine or a Glycine.

Ligand identification

We initially used OpenEye FRED to dock the substrate citrate against the hNaDC1 model (Figure 1), to guide ligand discovery with virtual screening. Similarly to citrate in the vcINDY structure, the carboxylate moieties of citrate are predicted to interact with the N-terminal SNT motif of hNaDC1 by forming hydrogen bonds with backbone atoms of Asn141 and Thr142, as well as with the hydroxyl moiety of the Ser140 sidechain. Citrate is

also coordinated by the sidechain hydroxyl of Thr519, the backbone nitrogen of Ala241, and Na⁺. The close similarity between the binding mode of citrate in the vcINDY crystal structure and the predicted binding mode of this weak inhibitor in the hNaDC1 model suggests that our models can predict binding of substrates or competitive inhibitors with substrate-like structures. We then virtually screened 2,726,001 compounds from various libraries of the ZINC database (Methods and Supplemental Data). 500 top-scoring hits from the various screens against the models of hNaDC1 and hNaDC3 were prioritized for experimental testing by visual analysis. In particular, top docking poses were inspected for erroneously-docked molecules, which can be observed in large virtual screenings, to remove molecules with incorrect ionization states, tautomers or strained conformations.^{32, 33} We then selected an initial set of eight molecules (compounds **1–8**, Table 1), based on their availability and the presence of unique chemical structure, as well as their interaction with confirmed key binding site residues, such as Ser143, Asn144, Thr245, and Thr485 in hNaDC3. These molecules contained dicarboxylates connected to various scaffolds. For example, compounds **2,4,5,6,7,8** contain 5- or 6-sided rings, and compounds **1,4,5,8** contain a nitrogen atom in a linear chain.

We tested the transport inhibition by the predicted ligands in a cis-inhibition assay against representative members of the SLC13 family, the human NaDC1, NaDC3 and NaCT, as well as the mouse NaDC1 and NaDC3. The transport substrates were [¹⁴C]succinate for NaDC1 and NaDC3 (both human and mouse) or [¹⁴C]citrate for the citrate transporter, NaCT. Four of the eight tested compounds (compounds **1, 3, 6, and 8**) significantly inhibited transport in at least one SLC13 family member (Figure 2 and Figure S1). Moreover, compound **1** inhibited [¹⁴C] substrate transport activity in all transporters, except for NaCT (Figure S1). The sensitivity to inhibition of hNaDC1 by compound **1** was somewhat variable and at the moment we do not have an explanation for this. Next, five additional molecules were selected from the ZINC database for experimental testing based on their similarity to our most potent hit compound **1** (compounds **9–13**, Table 1). These compounds were selected to refine the newly discovered scaffold of compound **1**, even though they were not necessarily ranked within the best 500 compounds of each screen (Table 1). Specifically, we focused on compounds with varying carbon chain length and diverse substituent size. For example, both **10** and **3** have benzene as a substituent, but the chains are four and five carbons long, respectively; both **6** and **11** have four carbon chains and two substituents, either two benzenes (**6**), or a benzene and a methyl group (**11**). All five compounds (**9–13**) inhibited at least one SLC13 member, with **10** being the most potent. Interestingly, hNaCT, which interacts with tricarboxylates such as citrate and exhibits unique substrate:stoichiometry, i.e. it binds four sodium ions, was significantly inhibited by compound **12**, a dicarboxylate with an aromatic moiety (Table 1; Figure S1).

Analysis of inhibitors

Based on the cis-inhibition assays, we compared the docking poses of compound **10**, one of the most potent inhibitors, in mNaDC1, and compound **3**, the most selective ligand for hNaDC3 inhibition (Figure 3). Both ligands are predicted to form hydrogen bonds with the conserved N- and C-terminal SNT motifs. Interestingly, subtle differences between the binding sites of these proteins may explain their differential binding specificities. For

example, Thr236 in mNaDC1 is substituted by Ala254 in hNaDC3 (Table S1; Figures 3A,B and 4A–D), leading to a formation of an additional subpocket by Leu59, Ile429 and Leu432 in hNaDC3. This subpocket can accommodate the bulky naphthalene moiety of compound **3** (Figure 3A,C). Moreover, in mNaDC1, the sidechain of Ile416 faces the binding site, making the corresponding pocket narrower, which limits the interaction with larger and bulkier ligands such as compound **3**.

Next, compounds **1** and **10** were selected for measurements of concentration dependent inhibition of hNaDC3, hNaDC1, and mNaDC1. These compounds were selected because (i) they were two of the most potent inhibitors among the 9 newly identified ligands, (ii) they exhibited some selectivity for specific SLC13 members (e.g., did not inhibit NaCT), and (iii) they differ in their lengths, where compound **1** and **10** are 5-atom and 4-atom chain dicarboxylates, respectively. mNaDC1 was inhibited by compound **1** with an IC₅₀ value of 72 μM (Figure 4A) and, in a second experiment (not shown), the IC₅₀ was 82 μM. hNaDC3 had higher IC₅₀ values compared with mNaDC1 (207 μM Fig. 4A, and in four experiments, 159 ± 41 μM). In contrast, hNaDC1 was insensitive to inhibition by compound **1** (Figure 4A). The results with compound **10** were similar to those with compound **1**. The IC₅₀ values for compound **10** were: mNaDC1 (85 μM (Figure 4B) and 100 μM, second experiment); hNaDC3 (59 μM (Figure 4B) and the mean of four experiments was 82 ± 14 μM). hNaDC1 was poorly inhibited by compound **10**, with an estimated IC₅₀ of ~2 mM. The IC₅₀ values for mNaDC1 and hNaDC3 are similar to their succinate K_m values.^{34, 35}

Next, we compared the predicted complexes of hNaDC3 and mNaDC1 with compounds **1** and **10**. Compound **1** adopts different binding modes in the two transporter/ligand complexes (Figure 5). In the hNaDC3 complex, compound **1** forms hydrogen bonds with sidechain atoms of the N- and C-terminal SNT motif residues and Van der Waals contacts in a hydrophobic subpocket, which is unique to this transporter (Figure 3A,C). Conversely, because the third position of the C-terminal SNT motif in mNaDC1 is occupied by a valine residue (Val471; Table S1), compound **1** interacts with the backbone atoms of the C-terminal SNT motif of this protein. Compound **10** exhibits similar differential mode of interaction across the two transporters, with one key difference. Compound **10** forms a hydrogen bond with the sidechain of Thr236 in mNaDC1, which is specific to this transporter (Figure 5D, Table S1). In summary, these newly identified inhibitors exhibited IC₅₀ values in the μM range and some selectivity, providing important chemical tools to further studying these transporters. Although not all the different specificities can be explained structurally at this point, the IC₅₀ values indicate that these newly discovered ligands can be physiologically and clinically relevant for membrane transporters found in the liver and kidney.^{9, 36}

DISCUSSION

Cellular concentrations of citric acid cycle (CAC) metabolites are partly determined by the activity of the SLC13 family of Na⁺-coupled di- and tricarboxylate transporters. Understanding the mechanisms of transport by this family is required for further characterization of their physiological roles, as well as for developing drugs against metabolic disorders and aging. A key step towards describing the substrate specificity

among the members of the SLC13 family includes structural characterization of these proteins, the identification of structure-function relationships within the family, and the discovery of novel, specific small molecule ligands for each. In this study, we took a modeling-based approach to identify new inhibitors of the SLC13 family, which represents an alternative to large-scale labor intensive inhibitor screens. This approach has been used successfully to identify ligands for several other transporters such as NET,³⁷ GAT-2,³⁸ and LAT-1.³⁹ Here we modeled mammalian SLC13 family members based on an inward conformation of vcINDY, the closest representative atomic resolution structure of this structural family. Although outward facing conformations can potentially be even more useful for inhibitor discovery, it has been previously proposed that vcINDY is an elevator-type transporter,¹⁸ in which the geometry of the binding site is similar for the different states of the transport cycle. This hypothesis is reinforced by our successful identification of inhibitors based on the inward facing models in this study.

Three key results are presented in this study. First, small molecule ligands for five SLC13 members from human and mouse (i.e., hNaDC1, mNaDC1, hNaDC3, mNaDC3, hNaCT) were identified at a high hit rate from structure-based virtual screening (Figure 2 and Figure S1; Table 1). This finding provides novel chemical tools to further characterize the cellular functions of these transporters. Second, optimization of the initial small molecule hits suggests that differential ligand binding specificity among SLC13 members is largely determined by the length of the carbon chain and size of the dicarboxylates (Table 1, Figures 2–4). This result provides preliminary tools for designing more specific chemical probes to further characterize the SLC13 members, as well as identifies lead-like molecules for future drug development. Third, systematic application of homology modeling of multiple SLC13 members, followed by ligand docking and experimental testing, as well as a comparison of their mode of interactions with their ligands, revealed key residues for function and selectivity (Figures 1,3,4; Table S1). This result visualizes key specificity determinants for this important family for the first time such as subpockets that can be targeted for the design of specific ligands. We now discuss each of the three findings in turn.

The first key finding from this study is the identification of novel, specific small molecule inhibitors for SLC13 members. All the newly discovered inhibitors contain aromatic rings that can be involved in previously uncharacterized interactions with hydrophobic binding site residues (e.g., with Leu59, Leu429, Leu432 in hNaDC3; Figure 3A,C). Because SLC13 members exhibit high substrate specificity, almost any change in the structure of a test compound may have large effects. Our results indicate the complexity of how ligand specificity is obtained in this family, where small changes on the binding site surface can shift the ligand preference. Notably, the newly identified inhibitors interact with SLC13 members with IC₅₀ values in the μM range, similar to physiological concentrations of substrates.³⁶ At present we do not know if the inhibitors only bind to the transporters or if they are transported themselves.

The second key result from this study is the optimization of our initial promiscuous hit (compound **1**) by testing new compounds with varying size and carbon chain length, which provide chemical features that can be further developed to pharmacophores targeting specific SLC13 members. Our previous docking of known substrates (e.g., succinate and

glutarate) against the hNaDC3 model suggested that such 4- or 5-carbon dicarboxylates may have various binding modes,²¹ which is in agreement with the predicted binding poses of compounds **1** and **10** in mNaDC1 in this study (Fig 5). For example, docking of compound **10**, with a 4-carbon dicarboxylate backbone, to hNaDC3 suggests that it forms hydrogen bonds with Thr485 of the C-terminal SNT motif (Figure 5; Table S1). In mNaDC1, this residue is substituted to a valine, and a different residue, Thr236 is predicted to contribute to the interaction with compound **10** by forming new hydrogen bonds with this compound (Figure 5D). However, molecular docking suggests that compound **1**, with a 5 carbon dicarboxylate backbone, is too large to rearrange itself and interact with Thr236. Compound **1** still inhibits mNaDC1, suggesting that the complexity of interaction between small molecules and SLC13 members is not entirely captured by modeling the inward conformation alone, as well as by using cell-based assays. Furthermore, only compound **12** had an effect on hNaCT, confirming the different inhibitor binding specificity of this transporter compared to the other members of the family.³⁰ These new ligands highlight the complexity of how the SLC13 members achieve their substrate specificity; despite the high similarity of their structures (they are all dicarboxylates and possess aromatic rings), their inhibition profiles are different. Future elucidation of SLC13 conformations as well as the application of complementary experimental approaches that directly measure binding and transport¹⁸ might explain this differential sensitivity to inhibition.

Third, our SLC13 models bound to previously and newly characterized ligands highlight two key positions that define a unique binding site in each SLC13 member, thereby providing a framework to rationalize substrate specificity among the SLC13 family members (Table S1). Position 1 is located in close proximity to the C-terminal SNT motif (Figures 1 and 5). For example, in hNaDC3 this residue (Ala254) contributes to the formation of an additional hydrophobic subpocket specific to this protein, that can accommodate bulkier ligands such as compound **3** (Figure 3A,C). Position 2 is the third residue of the C-terminal SNT motif, and it has some variability among the SLC13 members; it is occupied by a threonine residue in vINDY and NaDC3 (both human and mouse), or by a valine residue in NaDC1 (both human and mouse) and NaCT. As described in this study, this residue is likely to play a key role in interaction with ligands.

In conclusion, it is plausible that the combined differences among the transporters, although subtle, affect the overall hydrophobicity and shape of their corresponding binding sites, which is reflected in the binding specificities of their ligands. Some differences in inhibitor specificity between hNaDC3, mNaDC3 and hNaDC1, hNaCT could not be predicted by the models. Thus future experimental and computational characterization of SLC13 members and their homologs in additional conformations is likely to contribute to our understanding of transport mechanisms in this family. Taken together, this study shows the feasibility of using structure based approaches to identify potential inhibitors of the SLC13 family, and highlights the necessity of subsequent experimental verification. These findings are expected to inform future development of drugs targeting this family of transporters.

Supplementary Material

Refer to Web version on PubMed Central for supplementary material.

Acknowledgments

Funding statement:

This work was supported in part by the National Institutes of Health (R01 GM108911).

We thank P. M. Ung for technical assistance and maintenance of the computational resources required for this study. Thanks to D. Rozenshteyn for assistance with the inhibition experiments. This work was supported in part through the computational resources and staff expertise provided by the Department of Scientific Computing at the Icahn School of Medicine at Mount Sinai. We appreciate OpenEye Scientific Software Inc. for granting us access to its high-performance molecular modeling applications through its academic license program. This work was supported in part by the National Institutes of Health (R01 GM108911).

Abbreviations

SLC Transporters

Solute Carrier Transporters

References

- Gullans SR, Kone BC, Avison MJ, Giebisch G. Succinate alters respiration, membrane potential, and intracellular K⁺ in proximal tubule. *The American journal of physiology*. 1988; 255:F1170–1177. [PubMed: 3202180]
- Ruderman NB, Saha AK, Vavvas D, Witters LA. Malonyl-CoA, fuel sensing, and insulin resistance. *The American journal of physiology*. 1999; 276:E1–E18. [PubMed: 9886945]
- Stoppa GR, Cesquini M, Roman EA, Prada PO, Torsoni AS, Romanatto T, Saad MJ, Velloso LA, Torsoni MA. Intracerebroventricular injection of citrate inhibits hypothalamic AMPK and modulates feeding behavior and peripheral insulin signaling. *The Journal of endocrinology*. 2008; 198:157–168. [PubMed: 18469022]
- Rogina B, Reenan RA, Nilsen SP, Helfand SL. Extended life-span conferred by cotransporter gene mutations in *Drosophila*. *Science*. 2000; 290:2137–2140. [PubMed: 11118146]
- Wang PY, Neretti N, Whitaker R, Hosier S, Chang C, Lu D, Rogina B, Helfand SL. Long-lived Indy and calorie restriction interact to extend life span. *Proceedings of the National Academy of Sciences of the United States of America*. 2009; 106:9262–9267. [PubMed: 19470468]
- Fei YJ, Inoue K, Ganapathy V. Structural and functional characteristics of two sodium-coupled dicarboxylate transporters (ceNaDC1 and ceNaDC2) from *Caenorhabditis elegans* and their relevance to life span. *The Journal of biological chemistry*. 2003; 278:6136–6144. [PubMed: 12480943]
- Fei YJ, Liu JC, Inoue K, Zhuang L, Miyake K, Miyauchi S, Ganapathy V. Relevance of NAC-2, an Na⁺-coupled citrate transporter, to life span, body size and fat content in *Caenorhabditis elegans*. *The Biochemical journal*. 2004; 379:191–198. [PubMed: 14678010]
- Birkenfeld AL, Lee HY, Guebre-Egziabher F, Alves TC, Jurczak MJ, Jornayvaz FR, Zhang D, Hsiao JJ, Martin-Montalvo A, Fischer-Rosinsky A, Spranger J, Pfeiffer AF, Jordan J, Fromm MF, Konig J, Lieske S, Carmean CM, Frederick DW, Weismann D, Knauf F, Irusta PM, De Cabo R, Helfand SL, Samuel VT, Shulman GI. Deletion of the mammalian INDY homolog mimics aspects of dietary restriction and protects against adiposity and insulin resistance in mice. *Cell metabolism*. 2011; 14:184–195. [PubMed: 21803289]
- Pajor AM. Sodium-coupled dicarboxylate and citrate transporters from the SLC13 family. *Pflugers Arch*. 2014; 466:119–130. [PubMed: 24114175]
- Wright SH, Kippen I, Klinenberg JR, Wright EM. Specificity of the transport system for tricarboxylic acid cycle intermediates in renal brush borders. *The Journal of membrane biology*. 1980; 57:73–82. [PubMed: 7452725]
- Kekuda R, Wang H, Huang W, Pajor AM, Leibach FH, Devoe LD, Prasad PD, Ganapathy V. Primary structure and functional characteristics of a mammalian sodium-coupled high affinity dicarboxylate transporter. *The Journal of biological chemistry*. 1999; 274:3422–3429. [PubMed: 9920886]

12. Pajor AM, Gangula R, Yao X. Cloning and functional characterization of a high-affinity Na(+)/dicarboxylate cotransporter from mouse brain. *American journal of physiology Cell physiology*. 2001; 280:C1215–1223. [PubMed: 11287335]
13. Burckhardt BC, Drinkuth B, Menzel C, Konig A, Steffgen J, Wright SH, Burckhardt G. The renal Na(+)-dependent dicarboxylate transporter, NaDC-3, translocates dimethyl- and disulfhydryl-compounds and contributes to renal heavy metal detoxification. *Journal of the American Society of Nephrology: JASN*. 2002; 13:2628–2638. [PubMed: 12397032]
14. Schorbach L, Krick W, Burckhardt G, Burckhardt BC. Glutathione is a low-affinity substrate of the human sodium-dependent dicarboxylate transporter. *Nephron Physiology*. 2013; 124:1–5. [PubMed: 24247155]
15. Inoue K, Zhuang L, Ganapathy V. Human Na⁺-coupled citrate transporter: primary structure, genomic organization, and transport function. *Biochemical and biophysical research communications*. 2002; 299:465–471. [PubMed: 12445824]
16. Mancusso R, Gregorio GG, Liu Q, Wang DN. Structure and mechanism of a bacterial sodium-dependent dicarboxylate transporter. *Nature*. 2012; 491:622–626. [PubMed: 23086149]
17. Forrest LR, Kramer R, Ziegler C. The structural basis of secondary active transport mechanisms. *Biochimica et biophysica acta*. 2011; 1807:167–188. [PubMed: 21029721]
18. Mulligan C, Fitzgerald GA, Wang DN, Mindell JA. Functional characterization of a Na⁺-dependent dicarboxylate transporter from *Vibrio cholerae*. *The Journal of general physiology*. 2014; 143:745–759. [PubMed: 24821967]
19. Bolla JR, Su CC, Delmar JA, Radhakrishnan A, Kumar N, Chou TH, Long F, Rajashankar KR, Yu EW. Crystal structure of the *Alcanivorax borkumensis* YdaH transporter reveals an unusual topology. *Nature communications*. 2015; 6:6874.
20. Su CC, Bolla JR, Kumar N, Radhakrishnan A, Long F, Delmar JA, Chou TH, Rajashankar KR, Shafer WM, Yu EW. Structure and function of *Neisseria gonorrhoeae* MtrF illuminates a class of antimetabolite efflux pumps. *Cell reports*. 2015; 11:61–70. [PubMed: 25818299]
21. Schlessinger A, Sun NN, Colas C, Pajor AM. Determinants of substrate and cation transport in the human Na⁺/dicarboxylate cotransporter NaDC3. *The Journal of biological chemistry*. 2014; 289:16998–17008. [PubMed: 24808185]
22. Pei J, Kim BH, Grishin NV. PROMALS3D: a tool for multiple protein sequence and structure alignments. *Nucleic acids research*. 2008; 36:2295–2300. [PubMed: 18287115]
23. Shen MY, Sali A. Statistical potential for assessment and prediction of protein structures. *Protein Sci*. 2006; 15:2507–2524. [PubMed: 17075131]
24. Radestock S, Forrest LR. The alternating-access mechanism of MFS transporters arises from inverted-topology repeats. *Journal of molecular biology*. 2011; 407:698–715. [PubMed: 21315728]
25. Schlessinger A, Yee SW, Sali A, Giacomini KM. SLC classification: an update. *Clinical Pharmacology and Therapeutics*. 2013
26. Eramian D, Eswar N, Shen MY, Sali A. How well can the accuracy of comparative protein structure models be predicted? *Protein Sci*. 2008; 17:1881–1893. [PubMed: 18832340]
27. Pettersen EF, Goddard TD, Huang CC, Couch GS, Greenblatt DM, Meng EC, Ferrin TE. UCSF Chimera—a visualization system for exploratory research and analysis. *J Comput Chem*. 2004; 25:1605–1612. [PubMed: 15264254]
28. McGann M. FRED pose prediction and virtual screening accuracy. *J Chem Inf Model*. 2011; 51:578–596. [PubMed: 21323318]
29. Pajor AM, Randolph KM. Conformationally sensitive residues in extracellular loop 5 of the Na⁺/dicarboxylate co-transporter. *The Journal of biological chemistry*. 2005; 280:18728–18735. [PubMed: 15774465]
30. Pajor AM, Sun NN. Nonsteroidal anti-inflammatory drugs and other anthranilic acids inhibit the Na(+)/dicarboxylate symporter from *Staphylococcus aureus*. *Biochemistry*. 2013; 52:2924–2932. [PubMed: 23566164]
31. Pajor AM, Randolph KM. Inhibition of the Na⁺/dicarboxylate cotransporter by anthranilic acid derivatives. *Molecular pharmacology*. 2007; 72:1330–1336. [PubMed: 17715401]

32. Schlessinger A, Khuri N, Giacomini KM, Sali A. Molecular Modeling and Ligand Docking for Solute Carrier (SLC) Transporters. *Curr Top Med Chem*. 2013; 13:843–856. [PubMed: 23578028]
33. Shoichet BK. Virtual screening of chemical libraries. *Nature*. 2004; 432:862–865. [PubMed: 15602552]
34. Burckhardt BC, Lorenz J, Kobbe C, Burckhardt G. Substrate specificity of the human renal sodium dicarboxylate cotransporter, hNaDC-3, under voltage-clamp conditions. *American journal of physiology Renal physiology*. 2005; 288:F792–799. [PubMed: 15561973]
35. Pajor AM, Sun NN. Molecular cloning, chromosomal organization, and functional characterization of a sodium-dicarboxylate cotransporter from mouse kidney. *American journal of physiology Renal physiology*. 2000; 279:F482–490. [PubMed: 10966927]
36. Giacomini KM, Huang SM, Tweedie DJ, Benet LZ, Brouwer KL, Chu X, Dahlin A, Evers R, Fischer V, Hillgren KM, Hoffmaster KA, Ishikawa T, Keppler D, Kim RB, Lee CA, Niemi M, Polli JW, Sugiyama Y, Swaan PW, Ware JA, Wright SH, Yee SW, Zamek-Gliszczynski MJ, Zhang L. Membrane transporters in drug development. *Nature Reviews Drug Discovery*. 2010; 9:215–236. [PubMed: 20190787]
37. Schlessinger A, Geier E, Fan H, Irwin JJ, Shoichet BK, Giacomini KM, Sali A. Structure-based discovery of prescription drugs that interact with the norepinephrine transporter, NET. *Proceedings of the National Academy of Sciences of the United States of America*. 2011; 108:15810–15815. [PubMed: 21885739]
38. Schlessinger A, Wittwer MB, Dahlin A, Khuri N, Bonomi M, Fan H, Giacomini KM, Sali A. High Selectivity of the gamma-Aminobutyric Acid Transporter 2 (GAT-2, SLC6A13) Revealed by Structure-based Approach. *Journal of Biological Chemistry*. 2012; 287:37745–37756. [PubMed: 22932902]
39. Geier EG, Schlessinger A, Fan H, Gable JE, Irwin JJ, Sali A, Giacomini KM. Structure-based ligand discovery for the Large-neutral Amino Acid Transporter 1, LAT-1. *Proceedings of the National Academy of Sciences of the United States of America*. 2013; 110:5480–5485. [PubMed: 23509259]
40. Laskowski RA, Swindells MB. LigPlot+: multiple ligand-protein interaction diagrams for drug discovery. *Journal of chemical information and modeling*. 2011; 51:2778–2786. [PubMed: 21919503]

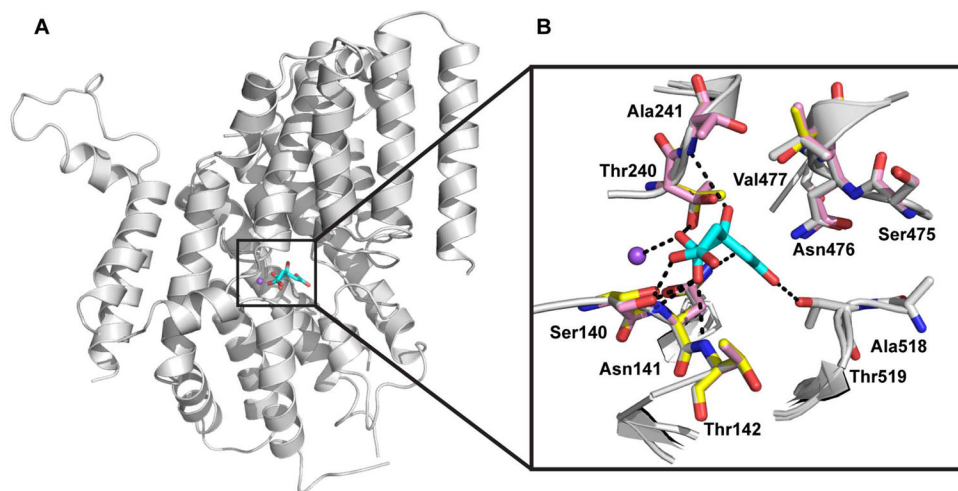


Figure 1. Homology models of the SLC13 transporters

(A) Docking pose of the known substrate citrate into the human NaDC1 (hNaDC1) homology model. The backbone atoms of hNaDC1 are visualized as white cartoon, and the ligand in cyan sticks, with oxygen, nitrogen, atoms in red, blue, respectively. The position of the sodium ion is derived from the model and represented as a purple sphere. (B) Comparison of the binding sites of the SLC13 transporters with hNaDC1 in white sticks, the mouse NaDC1 in pink and the human NaDC3 in yellow, with oxygen, nitrogen, atoms in red, blue, respectively. The hNaDC1 residues of the binding site are labeled and the position of the sodium ion derived from the model is represented as a purple sphere.

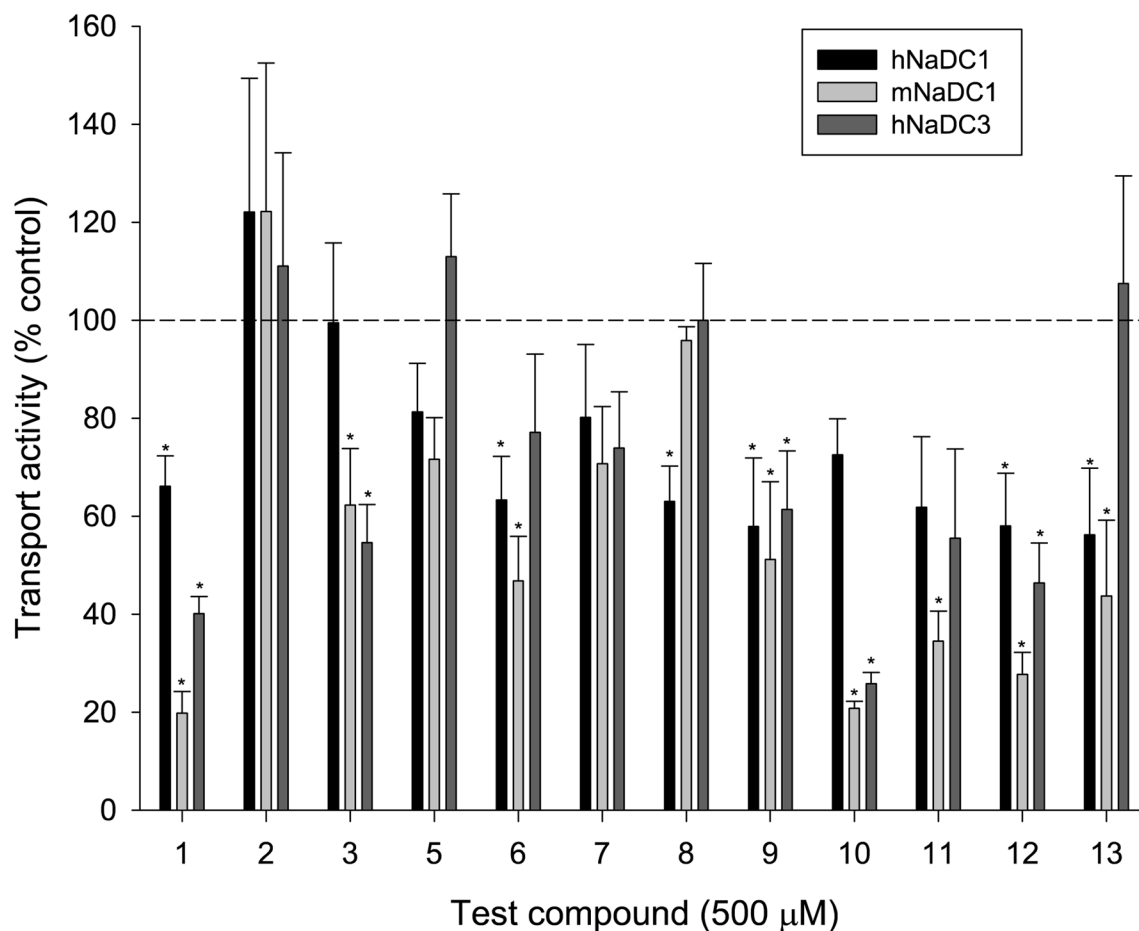


Figure 2. Experimental testing of predicted SLC13 inhibitors

HEK-293 cells expressing the following transporters were cultured in 96 well plates: human (h) or mouse (m) NaDC1, hNaDC3. *Cis*-inhibition of ~10 μM [¹⁴C]succinate transport was measured with 500 μM concentration of test compound, expressed as a percentage of transport in the absence of test compound (DMSO only). Error bars show the SEM (n=3–10 independent experiments). * denotes significant difference from control, P < 0.05. The dotted line indicates the position of 100%. Compound 4 had inconsistent effects and is not shown.

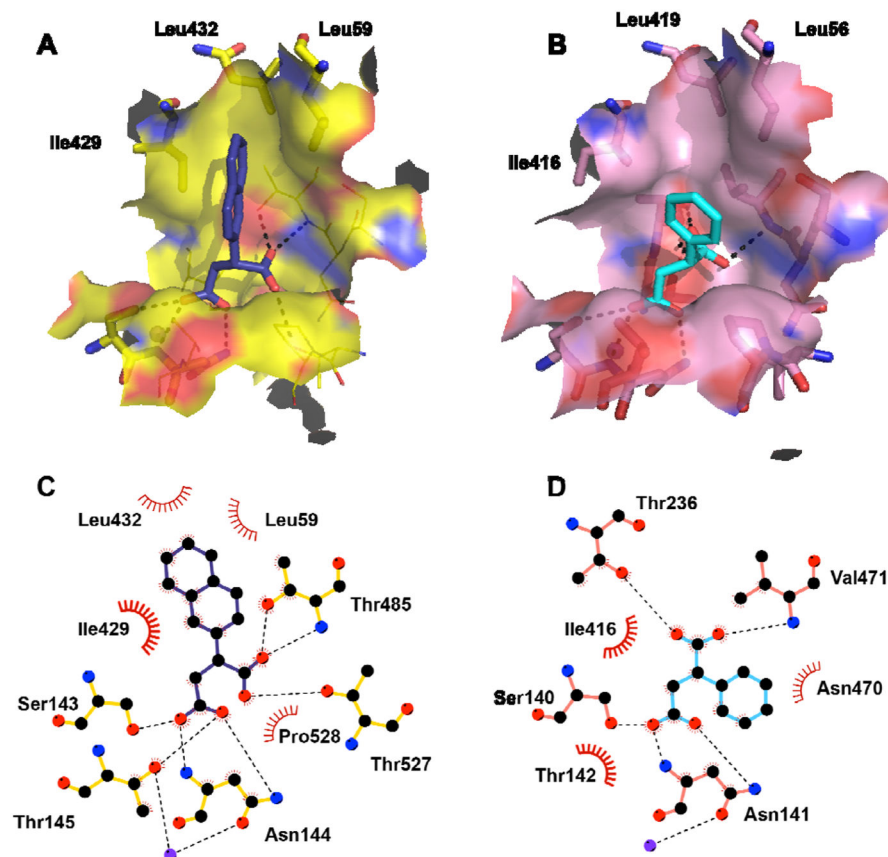


Figure 3. Mode of binding of newly discovered ligands

Docking poses of compounds **3** (Panels **A,C**) and **1** (Panels **B,D**) to the hNaDC3 and mNaDC1 binding sites respectively. The upper panels show the hNaDC3 (**A**) and mNaDC1 (**B**) binding sites in yellow and pink transparent surface respectively; The lower panels show the binding pose in a 2D representation generated by ligplot,⁴⁰ where the hNaDC3 (**A**) and mNaDC1 (**B**) residues forming hydrogen bonds with the ligands are represented in yellow and pink respectively, and the residues establishing hydrophobic contacts in red semi-circles. Compounds **3** and **10** are visualized as blue and cyan sticks, respectively.

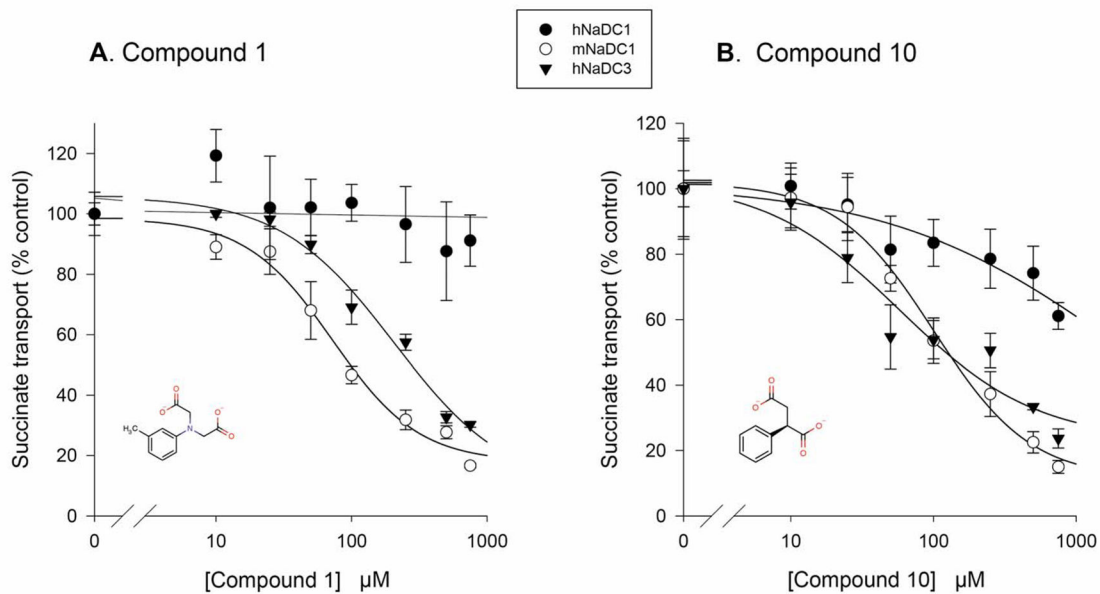


Figure 4. Concentration dependence of inhibition of SLC13 transporters by predicted SLC13 inhibitors

Transport of [^{14}C] succinate ($\sim 10 \mu\text{M}$) was measured in the presence and absence of test compound **1** (A) or **10** (B) at concentrations between 10 and 750 μM . HEK-293 cells were transiently transfected with plasmids encoding hNaDC1, mNaDC1 or hNaDC3. The data points are normalized to transport activity in the absence of inhibitor. Error bars represent SEM, $n=3$ wells from a single experiment.

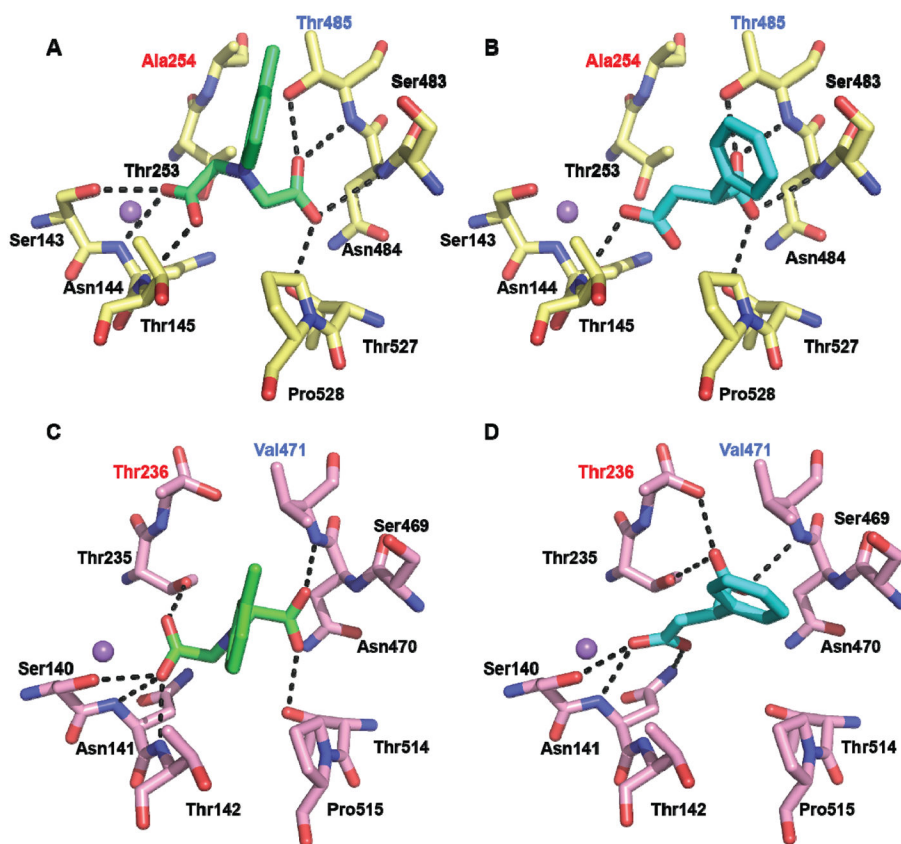
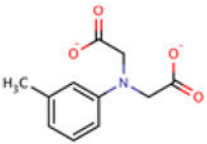
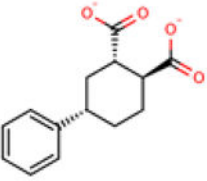
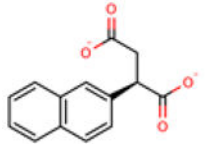
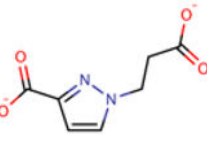
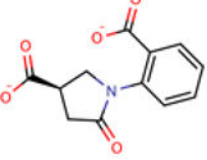
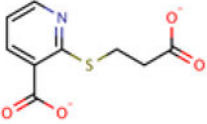
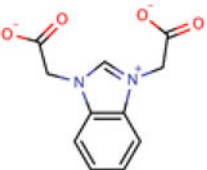
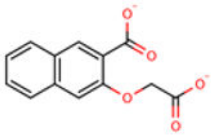
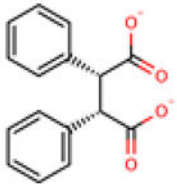
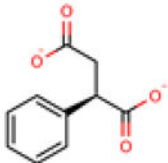
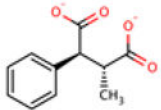
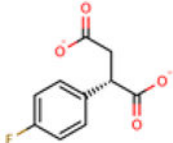
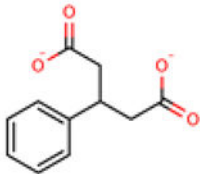


Figure 5. Predicted ligand binding mode for hNaDC3, mNaDC1
Docking poses of compounds **1** (A, C) and **10** (B, D) represented in hNaDC3 (yellow) and mNaDC1 (pink) respectively. Compounds **1** and **10** are represented in green, and cyan respectively, with oxygen atoms in red and nitrogen, atoms blue. Residues defining substitutions 1 and 2 (Table 1) are labeled in red and blue, respectively.

Table 1

Top-scoring compounds tested in uptake experiments

Compound ^a	Rank ^{b,c}	Sketch ^d
1	500+, 20	
2	500+, 33	
3	500+, 50	
4	500+, 80	
5	3, 1	
6	26, 93	
7	311, 178	

Compound ^a	Rank ^{b,c}	Sketch ^d
8	379, 40	
9	500+, 500+	
10	500+, 500+	
11	500+, 500+	
12	500+, 500+	
13	500+, 500+	

^aCompound gives the number for each molecule

^{b,c}Rank provides the rank of the compound within the virtual screening against the hNaDC1 (b) and hNaDC3 (c) models. 500+ indicates that the compound was not ranked within the 500 best scored compounds visually analyzed

^dSketch marks the 2D structure of the molecule